Photoacoustics 29 (2023) 100428

Contents lists available at ScienceDirect

Photoacoustics

journal homepage: www.elsevier.com/locate/pacs

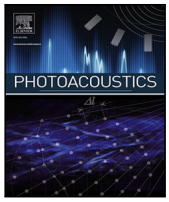

Photoacoustic methane detection inside a MEMS microphone

Thomas Strahl [a,b,*], Jonas Steinebrunner [b], Christian Weber [a,b], Jürgen Wöllenstein [a,b], Katrin Schmitt [a,b]

[a] Laboratory for Gas Sensors, Department of Microsystems Engineering, University of Freiburg, Georges-Köhler-Allee 102, Freiburg, 79110, Germany
[b] Department of Gas and Process Technology, Fraunhofer Institute for Physical Measurement Techniques IPM, Georges-Köhler-Allee 301, Freiburg, 79110, Germany

ARTICLE INFO

Keywords:
Gas sensing
Laser spectroscopy
Photoacoustic
MEMS microphone
Methane

ABSTRACT

An innovative laser based photoacoustic (PA) gas sensing concept with intrinsic miniaturization potential was developed and investigated for methane trace gas detection. An interband cascade laser (ICL) with an optical power of 8.5 mW targets a methane (CH_4) absorption line feature around 3057.7 cm^{-1} (or 3270 nm). The ICL was focused into the sound port of a MEMS microphone, where the PA signal was generated and detected using a wavelength modulation concept (2f-WMS-PAS). The MEMS microphone was successfully implemented as an intrinsically miniaturized PA cell being gas sensing volume, acoustic resonator and sound transducer at once. Frequencies between 2 kHz and 100 kHz were investigated and used for methane detection. A sensitive and resonant methane detection at 41.8 kHz was investigated by concentration variations between 0 and 10 ppm CH_4 in N_2. A limit of detection (3σ-LOD) of 329 ppb was estimated. The long term stability of this sensor was investigated by the measurement of methane in ambient air. A noise equivalent concentration (NEC) of 14 ppb (parts per billion) at an average time of 10 s was estimated. This value corresponds to a normalized noise equivalent absorption (NNEA) of $2 \cdot 10^{-8}$ W cm^{-1} $Hz^{-1/2}$. Using the MEMS microphone directly as PA cell offers the possibility for an extremely miniaturized, highly sensitive and very cost-efficient photoacoustic trace gas sensor.

1. Introduction

A highly miniaturized, cost-efficient and simple sensor design for trace gas sensing would have the potential for a widespread use. For instance, the monitoring of toxic and combustible gases for health or safety reasons (eg. leakages) and greenhouse gases (GHGs). In this context, methane (CH_4) is one of the most important and prominent representatives. CH_4 is colorless, odorless, non-toxic, highly flammable and potentially explosive between a volume concentration of 4.4% and 17% in air. Due to the fact that CH_4 is the main component of natural gas with approx. 90%, it is a major source for heat and electricity as well as for industrial and natural processes.

The latest IPCC report (Intergovernmental Panel on Climate Change) highlights the influence of CH_4 as GHG. Its contribution to global warming is estimated by 0.5 °C in comparison to preindustrial times. Apart from carbon dioxide (CO_2), CH_4 is the most important GHG that affects global warming. Between 1750 and 2019, contributions from emitted GHG to global surface temperature changes match with their anthropogenic effective radiative forcing (ERF) contributions. A large part of the total anthropogenic ERF of 2.72 W m^{-2} (increase from 1.96 to 3.48 W m^{-2} from 1750 to 2019) is estimated to the ERF of CH_4 with 1.21 W m^{-2}. This ERF increase in terms of CH_4 is predominantly driven by anthropogenic emissions and the atmospheric CH_4 concentration has increased about 156% in this period to 1.866 ppm (parts per million) in 2019. In the last decade (2010–2019), the CH_4 concentration growth was 7.6 ppb (parts per billion) per year. The largest natural CH_4 emissions are from wetlands, freshwater and geological process, while the largest anthropogenic CH_4 emissions are from enteric fermentation and manure treatment, landfills and waste treatment, rice cultivation and fossil fuel exploitation [1].

In this sense, the identification and quantification of methane emissions can be motivated by safety or environmental concerns as well as by legal, economic or research aspects. For instance, fugitive methane emissions from the U.S. oil and natural gas are well documented and show the need for sensor solutions [2,3]. However, the quantification of methane emissions by local concentration anomalies can be challenging since the released CH_4 will be generally strongly diluted by ambient air [4,5].

Methane shows a line spectrum with infrared active modes in the mid-infrared (MIR, fundamental stretching mode ν_3- and the bending

* Corresponding author at: Department of Gas and Process Technology, Fraunhofer Institute for Physical Measurement Techniques IPM, Georges-Köhler-Allee 301, Freiburg, 79110, Germany.
E-mail address: thomas.strahl@ipm.fraunhofer.de (T. Strahl).

https://doi.org/10.1016/j.pacs.2022.100428
Received 19 October 2022; Received in revised form 23 November 2022; Accepted 27 November 2022
Available online 1 December 2022

mode ν_4 around 3.3 μm and 7.6 μm, respectively), and an overtone band in the near-infrared (NIR, $2\nu_3$ around 1.65 μm). The fundamental modes in the MIR are around 100 times stronger than the overtone mode in the NIR in terms of absorption line strength [6].

Distributed feedback (DFB) lasers for the infrared wavelength regime are the best suited choice for trace gas sensing. Unique technical characteristics such as continuous wave (cw), single mode, narrow line width (eg. 5 MHz) emission, tunability over a few wavenumbers (eg. 5 cm^{-1}) as well as long lifetime, compactness, room-temperature operation or commercial availability pave the way for successful trace gas spectroscopy applications. These infrared lasers can be roughly divided into three types: diode lasers (DLs, < 3 μm), interband cascade lasers (ICLs, 3–6 μm) and quantum cascade lasers (QCLs, > 3 μm). Choosing a suitable laser for a specific gas absorption line (FWHM around 3 GHz or 0.1 cm^{-1} at STP)[1] allows trace gas concentration measurements down to ppm-, ppb- or even ppt (part per trillion) level in a selective manner.

Well established laser absorption spectroscopy schemes in the infrared show remarkable results but sensitive setups can only be realized with sufficient optical path length according to Beer–Lambert-Law. Consequently, multi-reflection cells as well as optical cavity concepts have been developed to increase the optical path length in a comparably small volume [7,8]. The drawback of these approaches is the complex sensor design including delicate optical alignment and appropriate components (mirrors, lenses, windows, detectors, etc.) [9–13]. In other words, the miniaturization potential for optical trace gas detection concepts is limited. Up to now, these devices are trapped in a niche market due to a lack of compelling and scalable miniaturization concepts in combination with complex sensor designs.

Based on the photoacoustic (PA) effect [14], an alternative gas sensing approach can be offered by laser-based photoacoustic spectroscopy (PAS). By light-matter interaction due to infrared-active gas molecules, the absorbed infrared light can generate pressure fluctuations (or sound waves, yielding the PA-signal) that correlates with the gas concentration [15,16]. In this case, the sensitivity of the PA sensor scales with the absorbed light intensity that offers a potential for miniaturization. In the last decades, gas sensing devices based on PAS have been investigated in various configurations and applications [17,18]. As a rule of thumb, the miniaturized photoacoustic cells can reduce the gas sampling volume up to 2 or 3 orders of magnitude compared to gas sampling cells of the above mentioned optical detection concepts (eg from few cm^3 to few mm^3 or several ml to several μl). Recently, various miniaturized photoacoustic cells with different sound wave detectors such as MEMS-microphones, quartz tuning forks (QTF, also QEPAS for quartz-enhanced PAS) or cantilevers have been successfully developed [19–25]. However, their potential for miniaturization is still developing and relies on technical progress combined with novel concepts.

In this paper, we investigate an idea promising of an intrinsic miniaturization, i.e. using a typical MEMS microphone as miniaturized PA cell for photoacoustic trace gas sensing. In this context, a brief description of the photoacoustic signal generation and detection within a MEMS microphone is given in the following section. For demonstration purposes, a mid-infrared interband cascade laser (ICL) is focused into the sound port into the microphone. The target gas can be also injected or diffusing through the sound port of the microphone as described in the third section (experimental setup). This simple sensor design was tested for methane trace gas detection in nitrogen and ambient air. The results are shown and interpreted in the results and discussion section. Finally, a conclusion is drawn at the end of this paper.

[1] FWHM, full width half maximum, STP standard temperature (296 K) and pressure (1013 mbar).

2. Photoacoustic signal generation and detection within a MEMS microphone

In detail, the generation of sound waves or the PA signal by the photoacoustic effect is described in the literature [15–18]. In a nutshell, the PA signal in a gas sample cell can be generated by periodically excited molecules due to modulated light absorption. As a result, a local periodic heating is induced by collisions as non-radiative relaxation process. These thermal fluctuations of the gas sample in a fixed volume produce periodic acoustic waves (pressure fluctuations or sound) that can be measured by a microphone. The amplitude of the acoustic wave can be referred to as PA signal that is directly proportional to the absorbed light intensity and therefore also proportional to the gas concentration and laser power. The sound generation and detection scheme will be further described after introducing the MEMS microphone as PA cell.

2.1. MEMS microphone as PA cell

The term PA cell is classically used for the gas sample cell as acoustic unit with or without resonator concept, buffer volumes, acoustic filters, windows, gas inlet and outlet as well as a microphone. In order to increase the sensitivity for gas sensing, the gas sample cell is often designed as acoustic resonator. In this work, a typical MEMS microphone is directly used as PA cell. Silicon-based MEMS microphones are nowadays mass-produced for consumer electronics. This microphone type operates similar to the principle of a plate capacitor. As illustrated in Fig. 1(a), sound can enter the microphone through a (bottom) sound port and drives a flexible membrane electrode against a rigid reference electrode (backplate). Applying a constant charge bias, a voltage change can be read out (analog or digital signal) by means of an ASIC (application-specific integrated circuit) according to the membrane displacement that induces a capacitance change. The signal (voltage change, i.e. membrane displacement) is dependent on the amplitude and frequency of the incoming sound. Common MEMS microphones are designed according to a desired linear amplitude and flat frequency response for the audio band between 20 Hz and 20 kHz as shown in Fig. 1(c). The design dependent resonance peak slightly above 20 kHz is formed by the Helmholtz resonator that origins from the air volume in front of the membrane (or front volume) and the sound port dimensions [26,27]. Above the Helmholtz resonance (ultrasound regime), the frequency response is not investigated or documented in common data sheets of MEMS microphones. In particular, the design of sound port and front volume motivates a first experimental investigation of using a typical MEMS microphone as gas sample cell, acoustic resonator and sound transducer at the same time for photoacoustic gas sensing. In this work or in contrast to classical PA cells, the MEMS microphone as PA cell is used without any additional designed or integrated buffer volumes, acoustic filters, optical elements such as windows, specific designed gas inlet and outlet.

2.2. Photoacoustic signal generation and detection scheme

According to the above described signal generation, the PA signal (S_{PA}) can be mathematically expressed by

$$S_{PA} \propto \Delta p \propto \Delta H \propto \Delta I_{abs} \quad , \tag{1}$$

where Δp and ΔH denote the temporal change of sound pressure and heat density respectively in the gas by a temporal change of the absorbed light (ΔI_{abs}). The absorbed light intensity can be approximated by $I_{abs} \approx \mathcal{A} \cdot I_0$, where I_0 represents the initial laser intensity. The absorbance $\mathcal{A}$ can be divided into a term of gas absorption $\mathcal{A}_g$ and a term of background absorption $\mathcal{A}_{bkg}$ ($\mathcal{A} = \mathcal{A}_g + \mathcal{A}_{bkg}$). Introducing a background absorption is needed since the laser is focused into the microphone and laser light will also be absorbed by parts of the microphone (membrane, cap, etc.). However, this significant background

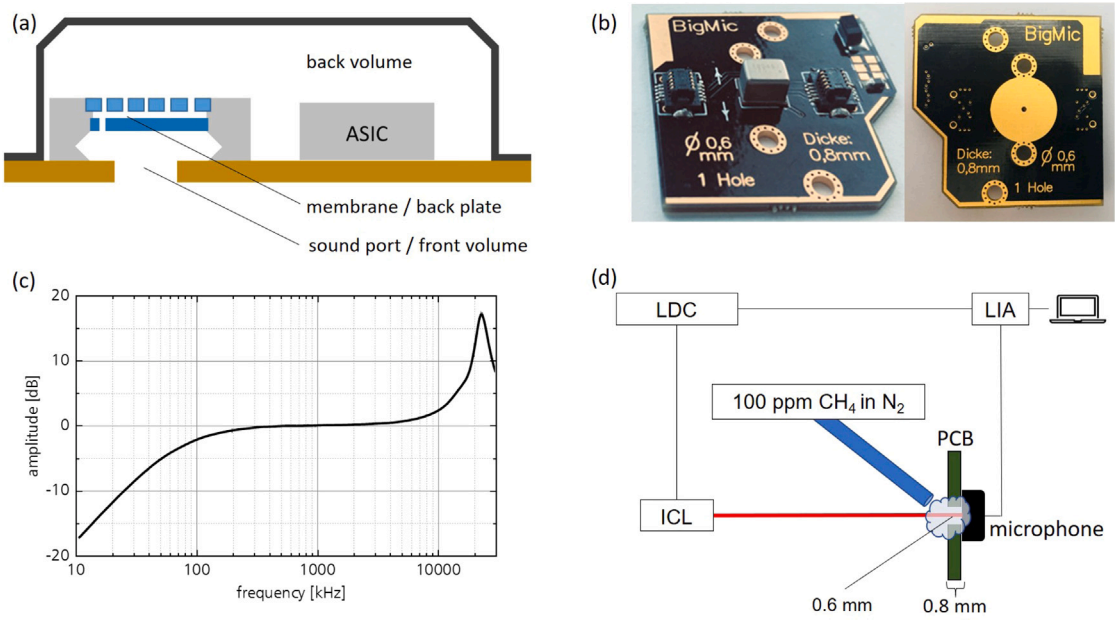

Fig. 1. (a) Schematic MEMS microphone package with bottom sound port. (b) Bottom port microphone with metal cap (TDK InvenSense, ICS-40730, 4.76 mm × 3.72 mm × 3.5 mm) soldered on a customized printed circuit board (PCB) with a thickness of 0.8 mm. The sound port of the microphone is aligned with the circular hole in PCB with a diameter of 0.6 mm. (c) Frequency response of typical MEMS microphones including the Helmholtz resonance above 20 kHz. (d) Schematic experimental setup of the photoacoustic gas sensor including interband cascade laser (ICL), MEMS microphone on the customized PCB as PA cell, laser diode controller (LDC) and lock-in amplifier (LIA).

absorption is assumed to be specially broad compared to the narrow gas absorption line (approx. 0.1 cm^{-1}).

In principle, intensity or wavelength modulation schemes (IM or WM) [16,28] can be applied to modulate the light absorption in order to generate the PA signal. Assuming a significant background absorption, a WM scheme in combination with a second harmonic detection (2f) is able to suppress or separate the background signal [29]. In consequence, the gas concentration (χ) correlates with the second harmonic (2f) WM-PAS signal (S_{PA}^{2f}) in a background free manner. Practically, S_{PA}^{2f} generated by a sinusoidal wavelength modulation (laser injection current modulation) around the absorption peak and 2f-lock-in detection scheme ($n = 2$):

$$\chi \propto S_{PA}^{nf} = \frac{1}{T}\int_{t-T}^{t} d\tilde{t} S_{PA}(\tilde{t}) \sin(2\pi n f \tilde{t}) \quad (2)$$

The laser modulation frequency is f and the acoustic frequency (f_s) of detected PA signal (S_{PA}^{nf}) corresponds to nth harmonic of this modulation frequency ($f_s = n \cdot f$) with $n = 2$ for the second harmonic. The integration time of the lock-in detection is denoted by T.

3. Experimental setup

The experimental setup in order to investigate the silicon MEMS microphone as miniaturized PA cell is shown in Fig. 1. A cw-DFB-ICL (Nanoplus) emitting at a wavelength of 3.27 µm is focused by a (collimation) lens through the sound port into the microphone. The microphone is low noise microphone with a signal to noise ratio of 74 dBA (TDK InvenSense, ICS-40730). It is a bottom port microphone and soldered on a customized printed circuit board (PCB) with a thickness of 0.8 mm. The sound port of the microphone is aligned with the circular hole in PCB with a diameter of 0.6 mm. The microphone dimensions are 4.76 mm × 3.72mm × 3.5mm. It is used as gas sample cell where the sound port is used as gas inlet/outlet. In order to vary the gas concentration in the PA cell, a gas tube with 4 mm diameter was placed close (few millimeters) to the orifice of the sound port without blocking the laser light.

The methane concentrations were varied between 0 and 100 ppm CH_4 in N_2 using mass flow controllers and two certified gas bottles

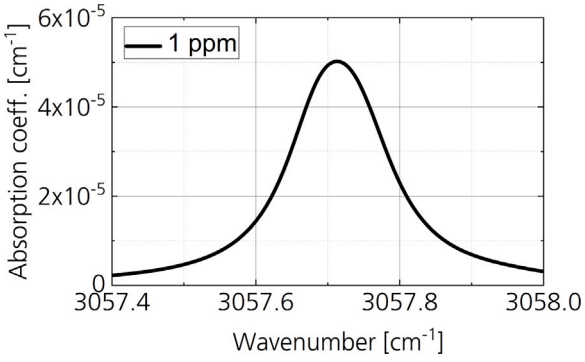

Fig. 2. Methane absorption around 3057.7 cm^{-1} (or 3270 nm). For 1 ppm CH_4 in N_2 at standard pressure and temperature (STP), the spectral absorption coefficient (in cm^{-1}) was calculated as a function of the wavenumber (in cm^{-1}) by HITRAN [6] parameters.

containing pure nitrogen (100% N_2 or so called zero gas) and 100 ppm CH_4 in N_2. During the measurement, the gas flux was kept constant at 300 ml/min. The laser targets the CH_4 absorption line around 3057.7 cm^{-1} (or 3270 nm) as shown in Fig. 2.

The ICL with a typical operation voltage of 5 V was driven by a commercial benchtop laser current driver and temperature controller (ILX Lightwave, LDC 3722). The laser (chip) temperature was adjusted to 20.70 °C and stabilized by means of peltier cooling (TEC). In general, an offset (or base, i_b) current of 78.15 mA was injected into the laser to tune its emission wavelength to the peak of the CH_4 absorption. Furthermore, the laser was wavelength and intensity modulated at a frequency (f) by an additional sinusoidal current of amplitude (i_{mod}) such that the injection current modulation is given by $i(t) = i_b + i_{mod} \cdot \sin(2\pi f t)$. The sinusoidal current was generated by a lock-in amplifier (LIA, Stanford Research Systems SR830) via the external modulation input of the current driver. The microphone signal was given into the LIA and demodulated at the 2nd harmonic (2f). The amplitude of the sine current was adjusted in order to maximize the 2f-PAS signal (S_{PA}^{2f}) at the peak absorption. The resonance behavior of PA cell was investigated by frequency scans. Therefore, the laser modulation

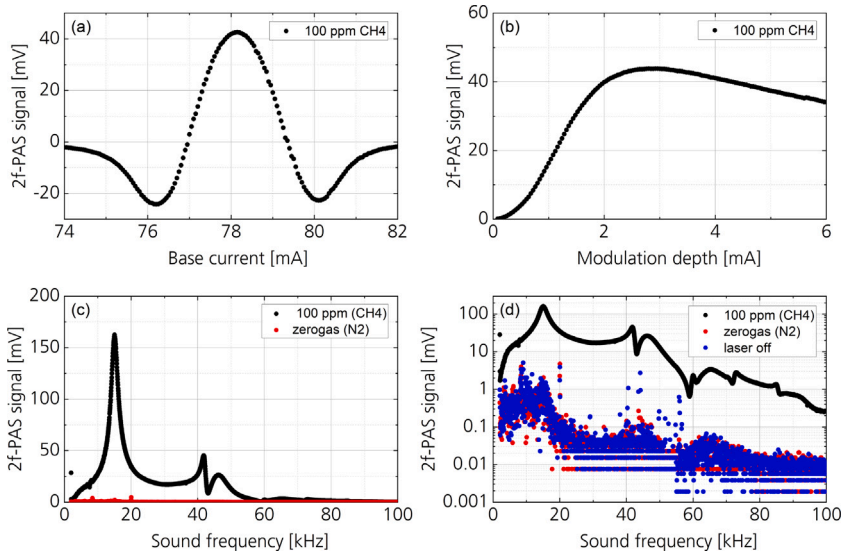

Fig. 3. (a) 2f-WMS-PAS signal (S_{PA}^{2f}) as function of base current (wavelength scan, i_b) is shown for 100 ppm CH_4 in N_2 at a fixed modulation frequency (f = 20.9 kHz) and modulation depth (i_{mod} = 2.4 mA). (b) 2f-PAS signal (S_{PA}^{2f}) as function of modulation depth (i_{mod}) is shown for 100 ppm CH_4 in N_2 at a fixed modulation frequency (f = 20.9 kHz) and base current (i_b = 78.15 mA). (c) The F-scan shows the 2f-PAS signal in dependence of the sound frequency ($f_s = 2f$) for 100 ppm CH_4 in N_2 and zero gas (100% N_2) at a fixed base current (i_b = 78.15 mA) and modulation depth (i_{mod} = 2.4 mA). (d) The shown F-Scans including an additional F-scan where the laser was turned off in logarithmic scale.

frequency (f) was swept from 1 to 50 kHz and the microphone signal was investigated at sound frequencies (f_s) between 2 and 100 kHz according to the presented 2f detection scheme ($f_s = 2f$). The LIA and its parameters were controlled by LabView software. The 2f-PAS signal was also recorded by LabView software on a PC. The integration time of the LIA was typically set to 300 ms in combination with a 3rd order low-pass filter. An optical power of around 8.5 mW was measured with the power meter (Thorlabs) at the given temperature and base current parameters.

4. Results and discussion

At first, it was demonstrated that the MEMS microphone has the ability to be used as PA cell for methane detection. This procedure also included the determination of suitable operation parameters for a sensitive methane detection. Furthermore, a more detailed PA sensor characterization at ppm-level was carried out for the selected parameters.

4.1. MEMS microphone as PA cell

A methane concentration of 100 ppm is used for the proof of principle and the characterization of resonant and non-resonant regimes in the following experiments.

Proof of principle

For the characterization of the microphone as PA cell, a methane flow is directed to the sound port of the microphone as described in the previous section. The gas detection in the 2f-WMS PAS concept depends crucially on a wavelength-modulated laser. More precisely, the parameters of the sinusoidal injection current $i(t) = i_b + i_{mod} \cdot \sin(2\pi f t)$ need to be carefully selected. The parameters (i_b, i_{mod} and f) can be iteratively optimized to maximize the 2f-PAS signal. The optimized parameters are shown in Fig. 3(a–c). Obviously, the MEMS Microphone can be used as PA cell for the laser based methane detection. The second derivative of the methane absorption around 3057.7 cm^{-1} can be obtained using a slow base current variation (wavelength scan) at a fixed modulation frequency and current amplitude (see Fig. 3(a)). The maximum of the 2f-PAS signal was obtained at the peak absorption (i_b = 78.15 mA at 3057.7 cm^{-1}) and the signal tends towards zero away from the absorption line. The current amplitude (wavelength modulation depth) was adjusted to i_{mod} = 2.4 mA at a fixed modulation frequency of f = 20.9 kHz (see Fig. 3(b)). It can be seen that without wavelength modulation takes place, no signal is generated since the gas absorption remains constant. On the other hand, the 2f-PAS signal decreases when the modulation depth is too large since less laser light is available for gas absorption. Based on the microphone design and the laser modulation concept, it might be possible to operate this PA cell in a resonant or non-resonant mode. The 2f-PAS signal as function of the laser modulation frequency f or sound frequency ($f_s = 2f$) at the peak absorption and optimized modulation depth is shown in the F-scan in Fig. 3(c). The PA signal difference in presence of methane or zero gas is obvious. In addition, the F-scan shows a remarkable functionality of the microphone beyond audio band. A PA signal as well as acoustic resonances were observed in the ultrasound regime in the presence of methane. Before characterizing the resonance in more detail, it can be clearly stated that this typical MEMS microphone can be used as gas sample volume, acoustic resonator and sound detector (commonly referred to as PA cell) at the same time for photoacoustic methane detection.

Characterization of resonant and non-resonant regimes

Three resonance peaks can be identified in Fig. 3(c) which are located at sound frequencies of 15.0, 41.8 and 46.3 kHz. The origin of the first resonance can be linked to the Helmholtz resonance of the microphone that is typically located slightly above 20 kHz [27]. This resonance was probably shifted to a lower frequency around 15 kHz by the combination of the customized PCB (eg. thickness and hole diameter) and microphone. The dimensions of the sound port and the front volume of the microphone were effectively changed and a shift to a lower Helmholtz resonance is likely due to the enlarged neck and front volume. Further investigations in order to confirm this explanation are beyond the scope of this work. Further resonances can be observed by plotting the 2f-PAS signal in a logarithmic scale (see Fig. 3(d)). However, more systematic investigations regarding the exact microphone structure and a modeling of the microphone as photoacoustic resonator would be required to understand the observations in more detail.

Nevertheless, a significant methane signal for 100 ppm can be observed over the full frequency scan up to 100 kHz. Towards higher

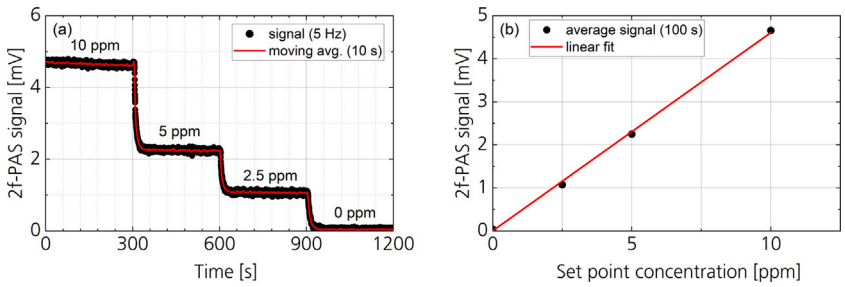

Fig. 4. (a) 2f-PAS signal (S_{PA}^{2f}) at a measurement rate of 5 Hz (black) and with a moving average of 10 s (red) is shown for several 5 min methane concentration steps (10, 5, 2.5 and 0 ppm CH_4 in N_2). (b) Averaged 2f-PAS signal (S_{PA}^{2f}) for each CH_4 concentration step against the set point concentration (black) and corresponding linear fit (red line).

Table 1
Comparison of the 2f-PAS signal (S_{PA}^{2f}) with 100 ppm CH_4 in N_2 (signal in mV) and 2f-PAS signal with 100% N_2 (background in mV) at different characteristic sound frequencies ($f_s = 2f$ in kHz) in resonant or non-resonant regimes (resonant Y/N). Based on the signal to background ratio (SBR, dimensionless) a figure of merit is calculated for the different characteristic sound frequencies.

Frequency f_s (kHz)	Resonant (Y/N)	Signal (mV)	Background (mV)	SBR -
15.0	Y	160.8	1.1	144
31.9	N	17.6	0.02	843
41.8	Y	45.4	0.04	985
46.3	Y	26.4	0.04	576
100	N	0.262	0.006	44

frequencies, the 2f-PAS signal of methane tends to decrease. This fact can be explained by a less efficient generation of photoacoustic waves since the relaxation of excited methane molecules at high modulation frequencies towards 100 kHz is not fast enough anymore. Another explanation would be a decreasing membrane frequency response in the ultrasound regime. So far the frequency response in the ultrasound regime is unknown (eg. not specified in the datasheet or literature). However, considering the strength of the 2f-PAS signal with 100 ppm CH_4 in N_2, the resonance in the audio regime (15.0 kHz) is several times higher than the resonances in the ultrasound regime (41.8 and 46.3 kHz). Remarkably, the 2f-PAS signal without methane (also referred to as 100% N_2, zero gas or background signal) is also several times higher in the audio band than in the ultrasound region. This background signal is mainly dominated by ambient noise in the lab. In general, an effect of the laser (turned off) could not be observed compared to zero gas signal where the laser is turned on. This is a remarkable result, since it shows that the MEMS microphone as PA in combination with the modulation concept allows a so called zero-background detection. In other words, the 2f-PAS signal directly corresponds to the energy absorbed in the sample. The best signal (CH_4) to background (N_2) ratios (SBR) could be observed beyond the audio band between 20 and 50 kHz where the ambient noise is significantly lower than in the audio band. Fig. 3(d) shows the fact that the largest SBR can be observed at the second resonance mode at 41.8 kHz in the ultrasound region (SBR of 985). The SBRs of the first three resonance modes and two characteristic non-resonant regimes around 32 and 100 kHz are documented in Table 1.

These values suggest that methane trace gas detection in the low-ppm regime is possible and even the detection of methane in ambient air should be possible.

4.2. Further performance characterization

In particular, the second resonance at 41.8 kHz seems most promising for sensitive methane measurements in the low-ppm regime (cf. SBR in Table 1). Consequently, the PA signal at 41.8 kHz (2nd resonance) for methane concentration in the low-ppm regime will be investigated in the following. Therefore, a fixed laser modulation frequency of 20.9 kHz ($f_s = 2f = 41.8$ kHz) was applied and the 2f-PAS signal analyzed.

Methane concentration variation

The sensitivity and linearity in terms of methane detection was tested by a stepwise methane concentration variation. The concentration was varied between 0, 2.5, 5 and 10 ppm CH_4 in N_2 within time intervals of 5 min. The 2f-PAS signal was recorded at a measurement rate of 5 Hz. The concentration steps are clearly visible (see Fig. 4(a)). The signal to noise ratio (SNR) can be significantly improved by a moving average of 10 s in post processing.

Calibration, linearity, sensitivity and limit of detection

The 2f-PAS signal (mV) can be transferred into methane concentration (ppm) by a sensor calibration. Therefore, an averaged 2f-PAS signal and the corresponding statistical uncertainty was calculated by 500 measurements or 100 s in the middle of each concentration step. As shown in Fig. 4(b), the averaged 2f-PAS signal scales linearly with the methane concentration. Consequently, a linear calibration curve can be calculated by a linear fit of the data set with $y = a + b \cdot x$. The linearity of the calibration curve is $R^2 \approx 0.999$. The sensor sensitivity (slope) was $b = (461 \pm 10)$ µV/ppm and the background level (intercept) $a = (3 \pm 50)$ µV. A limit of detection (LOD) can be estimated by the linear calibration curve and its parameters. To be more precise, the 3σ-LOD was calculated by the sensitivity or slope (b) and its uncertainty (σ_b) of the linear calibration according to $LOD(3\sigma) = 3\sigma_b/b = 0.329$ ppm. This 3σ-LOD is in line with Fig. 3 and suggests that methane in ambient air (around 1.866 ppm [1]) can be measured.

Accuracy, precision and long-term stability

For ambient air measurements, the gas flow through the tube was turned off such that ambient air can diffuse through the sound port into the microphone. A F-scan around the second resonance clearly shows that methane in ambient air can be detected as illustrated in Fig. 5(a). Additionally, the data offer that the best SBR is given at the resonance but it is shifted towards a lower frequency from 41.8 kHz for 100 ppm CH_4 in N_2 to 41.2 kHz for CH_4 in ambient air. This shift of 1.5% towards a lower resonance frequency (f_s) is in line by the slightly lowered speed of sound (c_s) or increased molecular weight (M) of the changed gas matrix ($f_s \propto c_s \propto 1/\sqrt{M}$). Besides nitrogen, ambient air also contains oxygen (approx. 20.9%) which needs to be taken into account. Carbon dioxide (approx. 400 ppm) and moisture (less than 1%) can be neglected in this context . In consequence, an adjustment of the laser modulation frequency to 20.6 kHz (= 41.2/2 kHz) is required to preserve the sensor calibration. An ambient air methane concentration around 1.6 ppm was calculated by applying the aforementioned sensor calibration on the 2f-PAS signal of ambient air at 41.2 kHz (see Fig. 5(b)). This value is below the expected methane concentration of ambient air of approx. 1.866 ppm (literature value [1]) but the residual between measurement and literature value is within two standard deviations as shown in Fig. 5(c). The corresponding error bars in terms of accuracy are calculated by error propagation ($\sigma_x = \sqrt{(\sigma_y/b)^2 + (\sigma_a/b)^2 + x^2(\sigma_b/b)^2}$) of the measured 2f-PAS signal (y) and the above described calibration ($y = a + bx$).

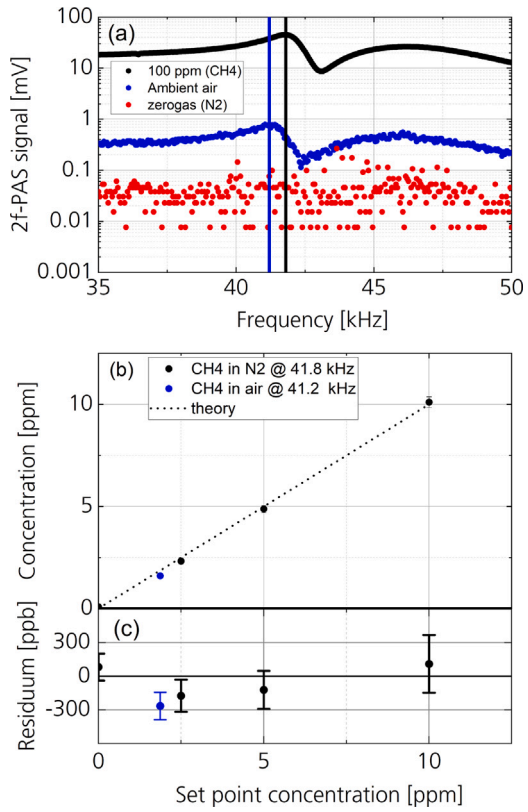

Fig. 5. (a) The F-scan (logarithmic scale) shows the 2f-PAS signal in dependence of the sound frequency ($f_s = 2f$) for 100 ppm CH_4 in N_2, CH_4 in ambient air and zero gas (100% N_2). (b) Comparison of the CH_4 concentration in N_2 and air with the set point concentrations (black and blue dots). The theoretical relation corresponds to a line from the origin with a slope of 1 (dashed line). (c) The residuals between measured and set point concentration are displayed with statistical errors.

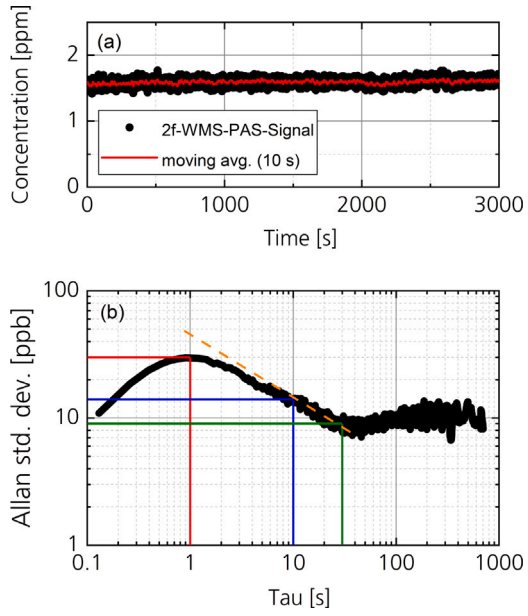

Fig. 6. (a) CH_4 concentration in air as a function of time. (b) Allan plot for the 50 min CH_4 concentration in air measurement.

The precision and the long-term stability (eg. drifts) of the measured concentration can be analyzed by means of an Allan–Werle plot. Based on a 50 min CH_4 in ambient air concentration measurement (see Fig. 6(a)), an Allan standard deviation can be calculated as shown in Fig. 6(b). The Allan standard deviation (in ppb) is shown as function of the (signal) average time (τ in s). For instance, the calculated standard deviation at $\tau = 1s$ and $\tau = 10$ s was given by 30 ppb and 14 ppb, respectively. Down to the minimum of the Allan–Werle Plot of 9 ppb around 40 s, the measurements are white noise dominated. This means that the Allan deviation generally follows a $1/\sqrt{\tau}$ trend line. For averaging times up to approx. 1 s, this $1/\sqrt{\tau}$ trend line is superimposed by an artifact of the integration time of the LIA that act as a low-pass filter [30]. Under these conditions, the Allan deviation gives an estimate for the precision of the measurement in the sense of a gaussian standard deviation that improves with averaging time, while the accuracy remains constant. In general, no significant drift could be observed during the 50 min measurement of CH_4 in ambient air. Consequently, the Allan deviation does not increase significantly for averaging times up to several hundreds of seconds. Overall, the sensor concept shows a remarkable stability. In addition, typical laser spectroscopic figures of merit can be derived from the Allan standard deviation such as the noise equivalent concentration (NEC) of 14 ppb at 10 s. The noise equivalent concentration or absorption (NEC in ppb and NEA in cm^{-1}) are derived from the Allan standard deviation at 10 s. This average time corresponds to a bandwidth of 0.1 Hz (inverse of the 10 s). For the normalized noise equivalent absorption (NNEA in W cm^{-1} $Hz^{-1/2}$), the NEA is divided by the square root of the bandwidth (0.1 Hz) and multiplied by optical laser power of 8.5 mW. These characteristic values are summarized in Table 2. These figures of merit as well as the estimated 3σ-LOD of 329 ppb are in the same order of magnitude as literature values of more complex laser-based PAS sensors concepts [4,20,31].

Table 2
Summary of figures of merit, noise equivalent concentration or absorption (NEC in ppb and NEA in cm^{-1} at an average time of 10 s) and normalized noise equivalent absorption (NNEA in W cm^{-1} $Hz^{-1/2}$).

NEC (ppb)	NEA (cm^{-1})	NNEA (W cm^{-1} $Hz^{-1/2}$)
14	$7 \cdot 10^{-7}$	$2 \cdot 10^{-8}$

5. Conclusion

An innovative laser-based photoacoustic gas sensing concept was developed and investigated for methane trace gas detection in the low ppm concentration range. An ICL with an emission wavelength of 2970 nm and an optical power of 8.5 mW was focused through the sound port into a MEMS microphone. This typical and commercially available MEMS microphone with dimensions of 4.76 mm × 3.72mm × 3.5mm was successfully tested as an intrinsically miniaturized PA cell. It was used simultaneously as gas sensing volume, acoustic resonator and sound transducer. The PA signal was generated by a WMS-2f modulation scheme and the methane detection was demonstrated in various ways (eg. wavelength scan, modulation amplitude scan or F-Scan). By means of F-Scans, the acoustically resonant and non-resonant regimes of the microphone as PA cell have been investigated between 2 and 100 kHz. Methane detection was demonstrated up to 100 kHz. In particular, a resonance at 41.8 kHz was investigated for a sensitive methane measurement between 0 and 10 ppm CH_4 in N_2 and CH_4 in ambient air. Furthermore, a 3σ-LOD of 329 ppb was estimated as well as a NEC of 14 ppb at an averaging time of 10 s. This value corresponds to a NNEA of $2 \cdot 10^{-8}$ W $cm^{-1}Hz^{-1/2}$. The 3σ-LOD is also an estimate for the accuracy that can probably be improved by a more sophisticated experimental setup. These results motivate further investigations in various directions. For instance, what kind of microphones work as PA cell, what happens with the light in the MEMS microphone exactly, investigation and simulation of the PA signal generation in the MEMS microphone, transfer of the concept to other gases by changing the

laser (wavelength) or use of another light source (LED). A full sensor miniaturization including laser and electronics is needed. The MEMS microphone as PA cell could offer a path for an extremely miniaturized, highly sensitive and very cost-efficient photoacoustic gas sensing device.

Funding

This project (“PaMeSan – Miniaturisierte laserbasierte Photoakustik zur Methan-Spurengasanalyse”) received financial support by Vector Foundation.

CRediT authorship contribution statement

Thomas Strahl: Idea and experimental design, Data analysis, Results interpretation, Writing the manuscript, Review. **Jonas Steinebrunner:** Experiments, Data analysis, Visualization, Review. **Christian Weber:** Electronic hardware, Results interpretation, Review. **Jürgen Wöllenstein:** Supervised the project, Review. **Katrin Schmitt:** Supervised the project and manuscript, Review.

Declaration of competing interest

The authors declare that they have no known competing financial interests or personal relationships that could have appeared to influence the work reported in this paper.

Data availability

Data will be made available on request.

Acknowledgments

Thanks to IPM colleagues Tobias Kolleth for the mechanical design, Eric Maier for LabView support and Armin Lambrecht for discussions and proof reading.

References

[1] P. Arias, N. Bellouin, E. Coppola, R. Jones, G. Krinner, J. Marotzke, V. Naik, M. Palmer, G.-K. Plattner, J. Rogelj, et al., Climate change 2021: The physical science basis. Contribution of working group14 I to the sixth assessment report of the intergovernmental panel on climate change; technical summary, 2021.

[2] R.A. Alvarez, S.W. Pacala, J.J. Winebrake, W.L. Chameides, S.P. Hamburg, Greater focus needed on methane leakage from natural gas infrastructure, Proc. Natl. Acad. Sci. 109 (17) (2012) 6435–6440.

[3] R.A. Alvarez, D. Zavala-Araiza, D.R. Lyon, D.T. Allen, Z.R. Barkley, A.R. Brandt, K.J. Davis, S.C. Herndon, D.J. Jacob, A. Karion, E.A. Kort, B.K. Lamb, T. Lauvaux, J.D. Maasakkers, A.J. Marchese, M. Omara, S.W. Pacala, J. Peischl, A.L. Robinson, P.B. Shepson, C. Sweeney, A. Townsend-Small, S.C. Wofsy, S.P. Hamburg, Assessment of methane emissions from the U.S. oil and gas supply chain, Science 361 (6398) (2018) 186–188.

[4] T. Strahl, J. Herbst, E. Maier, S. Rademacher, C. Weber, H.-F. Pernau, A. Lambrecht, J. Wöllenstein, Comparison of laser-based photoacoustic and optical detection of methane, J. Sens. Sens. Syst. 10 (1) (2021) 25–35.

[5] J. Chen, F. Dietrich, H. Maazallahi, A. Forstmaier, D. Winkler, M.E.G. Hofmann, H. van der Denier Gon, T. Röckmann, Methane emissions from the Munich Oktoberfest, Atmos. Chem. Phys. 20 (6) (2020) 3683–3696.

[6] I.E. Gordon, L.S. Rothman, C. Hill, R.V. Kochanov, Y. Tan, P.F. Bernath, M. Birk, V. Boudon, A. Campargue, K.V. Chance, B.J. Drouin, J.-M. Flaud, R.R. Gamache, J.T. Hodges, D. Jacquemart, V.I. Perevalov, A. Perrin, K.P. Shine, M.-A. Smith, J. Tennyson, G.C. Toon, H. Tran, V.G. Tyuterev, A. Barbe, A.G. Császár, V.M. Devi, T. Furtenbacher, J.J. Harrison, J.-M. Hartmann, A. Jolly, T.J. Johnson, T. Karman, I. Kleiner, A.A. Kyuberis, J. Loos, O.M. Lyulin, S.T. Massie, S.N. Mikhailenko, N. Moazzen-Ahmadi, H. Müller, O.V. Naumenko, A.V. Nikitin, O.L. Polyansky, M. Rey, M. Rotger, S.W. Sharpe, K. Sung, E. Starikova, S.A. Tashkun, J.V. Auwera, G. Wagner, J. Wilzewski, P. Wcisło, S. Yu, E.J. Zak, The HITRAN2016 molecular spectroscopic database, J. Quant. Spectrosc. Radiat. Transfer 203 (2017) 3–69.

[7] J. Hodgkinson, R.P. Tatam, Optical gas sensing: a review, Meas. Sci. Technol. 24 (1) (2013) 012004.

[8] Z. Du, S. Zhang, J. Li, N. Gao, K. Tong, Mid-infrared tunable laser-based broadband fingerprint absorption spectroscopy for trace gas sensing: A review, Appl. Sci. 9 (2) (2019) 338.

[9] C.R. Webster, G.J. Flesch, R.M. Briggs, M. Fradet, L.E. Christensen, Herriott cell spot imaging increases the performance of tunable laser spectrometers, Appl. Opt. 60 (7) (2021) 1958–1965.

[10] J.B. McManus, M.S. Zahniser, D.D. Nelson, J.H. Shorter, S.C. Herndon, D. Jervis, M. Agnese, R. McGovern, T.I. Yacovitch, J.R. Roscioli, Recent progress in laser-based trace gas instruments: performance and noise analysis, Appl. Phys. B 119 (1) (2015) 203–218.

[11] L. Tombez, E.J. Zhang, J.S. Orcutt, S. Kamlapurkar, W.M.J. Green, Methane absorption spectroscopy on a silicon photonic chip, Optica 4 (11) (2017) 1322.

[12] C.C. Teng, C. Xiong, E.J. Zhang, W.M.J. Green, G. Wysocki, Adaptive thermal stabilization of an integrated photonic spectrometer using parasitic interference fringes, Opt. Lett. 45 (12) (2020) 3252–3255.

[13] C.C. Teng, E.J. Zhang, C. Xiong, W.M.J. Green, G. Wysocki, Dynamic computational optical fringe mitigation in tunable laser absorption spectroscopy, Opt. Express 28 (26) (2020) 39017–39023.

[14] A.G. Bell, On the production and reproduction of sound by light, Am. J. Sci. s3-20 (118) (1880) 305–324.

[15] F.A. McDonald, G.C. Wetsel, Generalized theory of the photoacoustic effect, J. Appl. Phys. 49 (4) (1978) 2313.

[16] L.B. Kreuzer, The Physics of Signal Generation and Detection, Academic, New York, 1977, pp. 1–25.

[17] Z. Bozóki, A. Pogány, G. Szabó, Photoacoustic instruments for practical applications: Present, potentials, and future challenges, Appl. Spectrosc. Rev. 46 (1) (2011) 1–37.

[18] A. Miklós, P. Hess, Z. Bozóki, Application of acoustic resonators in photoacoustic trace gas analysis and metrology, Rev. Sci. Instrum. 72 (4) (2001) 1937–1955.

[19] J.-G. Coutard, A. Glière, J.-M. Fedeli, O. Lartigue, J. Skubich, G. Aoust, A. Teulle, T. Strahl, S. Nicoletti, M. Carras, et al., Photoacoustic cell on silicon for mid-infrared QCL-based spectroscopic analysis, in: MOEMS and Miniaturized Systems XVIII, Vol. 10931, SPIE, 2019, pp. 193–203.

[20] P. Patimisco, G. Scamarcio, F.K. Tittel, V. Spagnolo, Quartz-enhanced photoacoustic spectroscopy: a review, Sensors (Basel, Switzerland) 14 (4) (2014) 6165–6206.

[21] S. Palzer, Photoacoustic-based gas sensing: A review, Sensors (Basel, Switzerland) 20 (9) (2020) 2745.

[22] D. Pinto, H. Moser, J.P. Waclawek, S. Dello Russo, P. Patimisco, V. Spagnolo, B. Lendl, Parts-per-billion detection of carbon monoxide: A comparison between quartz-enhanced photoacoustic and photothermal spectroscopy, Photoacoustics 22 (2021) 100244.

[23] V. Koskinen, J. Fonsen, K. Roth, J. Kauppinen, Progress in cantilever enhanced photoacoustic spectroscopy, Vib. Spectrosc. 48 (1) (2008) 16–21.

[24] T. Tomberg, M. Vainio, T. Hieta, L. Halonen, Sub-parts-per-trillion level sensitivity in trace gas detection by cantilever-enhanced photo-acoustic spectroscopy, Sci. Rep. 8 (1) (2018) 1848.

[25] J.-G. Coutard, A. Berthelot, A. Glière, H. Lhermet, B. Scherer, T. Strahl, A. Teulle, T. Verdot, Micro PA detector: pushing the limits of mid IR photoacoustic spectroscopy integrated on silicon, in: Silicon Photonics XV, Vol. 11285, SPIE, 2020, pp. 179–187.

[26] A. Dehé, Silicon microphone development and application, Sensors Actuators A 133 (2) (2007) 283–287.

[27] A. Dehé, M. Wurzer, M. Füldner, U. Krumbein, The infineon silicon MEMS microphone, in: Proceedings Sensor 2013, 2013, pp. 95–99.

[28] S. Schilt, L. Thévenaz, Wavelength modulation photoacoustic spectroscopy: Theoretical description and experimental results, Infrared Phys. Technol. 48 (2) (2006) 154–162.

[29] C. Dewey, Design of Optoacoustic Systems, Academic, New York, 1977, pp. 47–76.

[30] P. Werle, Accuracy and precision of laser spectrometers for trace gas sensing in the presence of optical fringes and atmospheric turbulence, Appl. Phys. B 102 (2) (2011) 313–329.

[31] P. Patimisco, A. Sampaolo, L. Dong, F.K. Tittel, V. Spagnolo, Recent advances in quartz enhanced photoacoustic sensing, Appl. Phys. Rev. 5 (1) (2018) 011106.

Thomas Strahl, M.Sc studied physics at the University of Freiburg and at the Imperial College London (2009–2015). After his M.Sc. Degree in 2015, he joined the department for Gas and Process Technology at Fraunhofer Institute for Physical Measurement Techniques (IPM) in Freiburg. As research and development scientist, he focuses on signal processing for industrial laser spectroscopy applications. Since 2020, he is also a PhD student at the Laboratory for Gas Sensors at the Department of Microsystems Engineering, University of Freiburg.

Jonas Steinebrunner, B.Sc. is studying Microsystems Engineering for a M.Sc. Degree at the University of Freiburg (2015–2023). For his bachelor thesis, he joined the department for Gas and Process Technology at Fraunhofer Institute for Physical Measurement Techniques (IPM) in Freiburg as scientific assistant in 2019. His current research activity (master thesis) is focused on the development of methane trace gas sensors based on photoacoustic spectroscopy.

Christian Weber, M.Sc. studied Microsystems Engineering at the University of Freiburg from 2009 to 2016. After receiving his master's degree, he joined the department for Gas and Process Technology at Fraunhofer Institute for Physical Measurement Techniques (IPM) in 2016. His main focus concentrates on photoacoustic measurement systems, including the optical and acoustic design thereof as well as mixed signal electronic designs. In 2019, he also joined the Laboratory for Gas Sensors at the Department of Microsystems Engineering at the University of Freiburg as a PhD student.

Jürgen Wöllenstein, Prof. Dr. received his degree in Electrical Engineering from the University of Kassel in 1994. In 1994 he joined the chemical sensors group at the Fraunhofer Institute for Physical Measurement Techniques in Freiburg, where he is currently leading the department for Gas and Process Technology. In 2009, he became a Full Professor for Gas Sensors at the Department of Microsystems Engineering of the University of Freiburg.

Katrin Schmitt, Dr. studied physics at the Julius-Maximilians-University Würzburg and the University of Texas in Austin, USA (1999–2003). She received her PhD from the University of Strasbourg, France, in 2006 and since then is senior scientist at the Fraunhofer Institute for Physical Measurement Techniques in Freiburg. Since 2018 she is group leader at the Chair for Gas Sensors at the Department of Microsystems Engineering of the University of Freiburg.